IEEE Access
Multidisciplinary | Rapid Review | Open Access Journal

Received May 17, 2021, accepted June 6, 2021, date of publication July 1, 2021, date of current version July 12, 2021.

Digital Object Identifier 10.1109/ACCESS.2021.3094120

A Temperature Compensation Approach for Dual-Mass MEMS Gyroscope Based on PE-LCD and ANFIS

HUILIANG CAO[1], (Member, IEEE), WENQIANG WEI[1], LI LIU[2], TIANCHENG MA[1], ZEKAI ZHANG[1], WENJIE ZHANG[1], CHONG SHEN[1], AND XIAOMIN DUAN[3]

[1]Science and Technology on Electronic Test and Measurement Laboratory, North University of China, Taiyuan 030051, China
[2]Mechanized Infantry Reconnaissance Department, The Army Infantry Academy of PLA, Shijiazhuang 050083, China
[3]School of Electronic Science and Engineering, University of Electronic Science and Technology of China, Chengdu 611731, China

Corresponding authors: Tiancheng Ma (matiancheng1999@163.com) and Xiaomin Duan (dxm@uestc.edu.cn)

This work was supported in part by the National Natural Science Foundation of China under Grant 51705477, in part by the Aeronautical Science Foundation of China under Grant 2019080U0002, in part by the Key Research and Development (R&D) Projects of Shanxi Province under Grant 202003D111004, and in part by the Shanxi 1331 Project Key Subjects Construction.

ABSTRACT Because the dual-mass MEMS gyroscope's output is greatly influenced by temperature, which can lead to errors that cannot be ignored. To solve this problem, a novel compensation method is proposed: a parallel processing algorithm, which integrates the Permutation entropy (PE), Local Characteristic-scale Decomposition (LCD) and Adaptive network-based fuzzy inference system (ANFIS). Firstly, LCD is used to decompose the output which contains temperature noises and drifts into a trend component and several intrinsic scale components (ISC), according to autocorrelation and complexity, three different categories will be obtained by PE: pure noise output, mixed output, and drift output. The different processes are as follows, the noise output is discarded, the mixed output is filtered by SG (Savitzky-Golay filter), then dual ANFIS is applied. Since the drift output completely reflects the temperature characteristics, the degree of non-linearity is high, the ANFIS with complex rules is used for processing. And the mixed output is composed of intermediate layer modes, containing a relatively small amount of temperature characteristics, simple rule ANFIS is adopted for processing. Finally, the signal is reconstructed. After that, the temperature error experiment is carried out, the result shows the method can effectively eliminate the error and compensate for the drift, it has a fast convergence speed and good effect, and has the advantage of good compensation efficiency.

INDEX TERMS MEMS gyroscope, compensation, permutation entropy (PE), local characteristic-scale decomposition (LCD), adaptive network-based fuzzy inference system (ANFIS).

I. INTRODUCTION

A microelectromechanical system (MEMS) gyroscope is an angular velocity sensor based on the Coriolis force, it has low power consumption, small size, high performance, good stability, and it is broadly applied in many fields. The application area including altitude controlling, car and railway safety and navigation, intelligent weapons, micro position, navigation and timing system, wearable devices, industrial controlling system, aerospace systems, inertial navigation, consumer electronics and so on [1]–[5]. However, the temperature characteristics of MEMS gyro are always an important factor affecting the accuracy and performance [6], therefore, reduce the gyro temperature errors is very necessary, many works of literature are dedicated to this.

These techniques can be divided into hardware and software to compensate for temperature errors. The hardware compensation method is by designing the hardware configuration and control circuit, thereby reducing the gyro output error. For example, Cao *et al.* [7] established a new equivalent circuit model based on silicon structure at a high temperature such that the accuracy of the gyroscope has been improved, the performance becomes more stable. Fu *et al.* [8] designed a new circuit and proposed a simpler practical

The associate editor coordinating the review of this manuscript and approving it for publication was Gautam Srivastava.

effect model of temperature compensation to reduce the influence of resonance frequency and damping coefficient and improve the temperature characteristics of the gyroscope. Yang *et al.* [9] proposed a new temperature compensation structure of micro-gyroscope, which uses its on-chip temperature sensor and heater to control the temperature to achieve the compensation effect, the results show that it has a good effect, the temperature coefficient has been greatly optimized (3.95 times for scaling factor, 3.49 times for zero offset coefficient). Hardware compensation has achieved good results, but it costs a lot of money. The other is software compensation, that is, the output signal is processed by signal processing and mathematical model to eliminate the temperature error. The MEMS gyroscope's temperature characteristics are mainly composed of two parts, namely, low-frequency drift and high-frequency noise, the temperature error compensation needs to eliminate both of them.

Serial processing is a common method in software compensation [10]. Firstly, the output signal is denoised by using a filter, secondly, the drift is compensated by using the established mathematical model. The serial method has been widely used, but it is easy to destroy the low-frequency components and lose the effective components. So parallel processing is necessary, it can extract the high-frequency noise and low-frequency drift of the signal to different scales for different processing and reconstruction, which can greatly improve the efficiency of compensation [11]. For example, Shen *et al.* proposed a parallel model combining BEEMD (bounded ensemble empirical mode decomposition) and ELM (Extreme learning machine) to deal with the temperature error of MEMS gyroscope, which has a high accuracy [11]. In [12], a model based on EMD (empirical mode decomposition) and SVM (support vector machine) is proposed to compensate for the temperature error of the dynamically tuned gyroscope (DTG), after compensation, the average drift of the DTG is 0.0029 °/h, which is a successful drift modeling. In [13], to solve the long-term drift of gyro (CRG20) and improve the adaptability of gyro, a hybrid algorithm based on extreme learning machine (ELM) is proposed, and a good temperature compensation effect is obtained, the experimental result shows that the zero-bias index changes from 0.2779 °/s to 0.0046 °/s, and the random walk index changes from 0.0046 °/s/$\sqrt{\text{Hz}}$ to 5.94×10^{-4}°/s/$\sqrt{\text{Hz}}$.

The signal of the gyroscope changes nonlinearly with the temperature, and the error is similar to that of white noise. For the high-frequency noise part, the commonly used multi-scale analysis methods are WT (wavelet transform), EMD, and LMD (local mean decomposition) [14], [15]. WT is a common time-frequency analysis tool, which is often used in comprehensive denoising, but it lacks certain adaptability when the initial SNR (signal-noise ratio) of the signal is small, EMD has a better analysis effect, but there is modal aliasing in EMD. Therefore, many works of literature have studied the improved EMD algorithm, such as EEMD (ensemble empirical mode decomposition), CEEMDAN (Complete Ensemble Empirical Mode Decomposition with Adaptive Noise), etc. [16], [17], which to some extent suppresses modal aliasing, but there are still some problems, such as white noise is difficult to control. LMD is a non-stationary and non-linear signal processing method proposed by Jonathan S. Smith, by defining the connection curve in the way of moving average, the fitting error in EMD can be avoided, and the envelope signal and pure frequency modulation signal can be obtained automatically by decomposition. However, LMD itself has problems such as signal mutation, endpoint effect, and a large amount of calculation. Here, this paper applied the LCD algorithm, LCD decomposition is an adaptive time-frequency analysis method, which is proposed on the basis of EMD and LMD [18], [19] and applies to the analysis and processing of non-linear non-stationary signals. It can decompose complicated non-stationary signals into a series of single components with physical significance, which has high calculation efficiency and it has some advantages in the ability to suppress mode aliasing and end-point effect [20]. PE is a function to detect a sequence's complexity, it can magnify small quantities and is very sensitive to the changes in sequence, can analyze non-linear sequences well [21], [22]. Through the analysis of various modal components by PE, we can get the complexity information of modes, to carry out parallel processing.

The modeling of low-frequency drift is an important part of software compensation, it is very popular to use machine learning algorithms. For example, in [23], to solve the problem of temperature errors of fiber optic gyroscope, Chen proposed a genetic algorithm based on the Elman network, and the temperature drift problem is solved effectively. Song *et al.* used a novel fusion algorithm artificial fish swarm algorithm and backpropagation (BP) neural network model, and it is used to deal with the fiber optic gyroscope's drift characteristics influenced by temperature [24]. Chong *et al.* proposed a multiple-input single-output model based on Elman Neural Networks and Genetic Algorithm, a plurality of temperature variations can better describe temperature feature, increasing the effective dimensions of the model inputs [25]. In this paper, ANFIS is proposed [26], [27], the neural network is given fuzzy input signal and fuzzy weight, it is an effective fusion of neural network learning algorithm and the fuzzy system's language reasoning to make up for each deficiency, which has the characteristics of convenience and efficiency and has a good prediction effect. This paper will describe it in detail.

II. STRUCTURE AND DETECTION SYSTEM OF GYROSCOPE

A. STRUCTURE OF DUAL-MASS MEMS GYRO

The gyro studied in this paper is based on the principle of tuning-fork. As is shown in Figure 1, the structure includes two modes which are drive mode and sense mode, the drive mode includes three types: drive comb, driving springs, and driving frame, the sense mode also includes three types: sense comb, sense springs, and sense frame. It can be seen from the structure diagram that the structure of the two modes is separated, so there is no coupling displacement between the

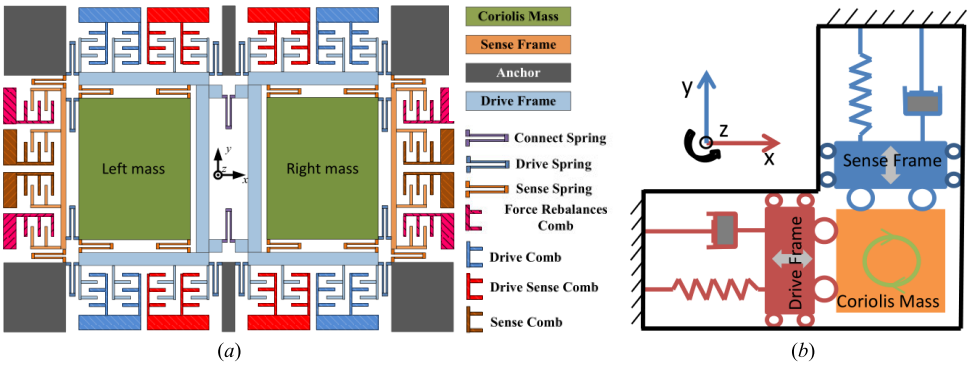

FIGURE 1. (a) Dual-mass MEMS gyro structure; (b) Gyro mechanical model.

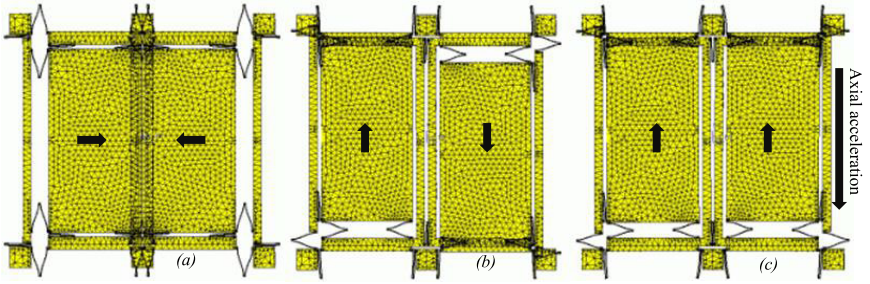

FIGURE 2. The working modes of the gyroscope (a) Drive mode; (b) Sense mode with Coriolis force; (c) Sense mode with axial acceleration.

two modes. In addition, the two masses are in the common part of the two modes, the effect of the mass of this common part is to generate vibration when there is an electrostatic drive. Once there is an electrostatic force, the left mass and the right mass will vibrate in the opposite direction of the x-axis. With the increase of the angular velocity in the z-axis, when it reaches a certain value Ω_z, the sense frame in the y-axis will detect the generated and transmitted Coriolis force, and the whole process will be monitored by the measurement and control circuit [28], [29].

Tuning fork theory is the principle of this structural drive mode. The left and right mass blocks are connected by U-shaped springs, the drive spring's x-axis is twisted to couple the two sensing masses. As shown in Figure 2, the modes have been simulated by Ansys software, the actual working drive mode is regarded as a pure inverting mode (fourth mode) for the following reasons: one is the structure's driving mode, the other is that the quality factor Q_{x2} of reverse drive mode is far greater than 2000, and thirdly, the frequency difference between the reverse phase and normal driving mode is relatively large (>1000 Hz). Since the second and third modes of the gyroscope constitute the actual working sense mode, in the ideal condition, the structural motion equation is expressed as:

$$m\ddot{S} + a\dot{S} + bS = E \tag{1}$$

Here, $S = [x, y_1, y_2]^{\mathrm{T}}$ is the displacement, x represents the drive mode's displacement, y_1, y_2 represent the sense in-phase and anti-phase mode's displacement, $m = [m_x, m_y, m_y]^{\mathrm{T}}$ is the mass, m_x is drive mode equivalent mass, m_y is sense mode quality, a and b are the damping coefficient and stiffness respectively, $E = [E_d \sin(\omega_d t), -2m_c\psi_z\dot{x}, -2m_c\psi_z\dot{x}_z]^{\mathrm{T}}$ is the external force matrix, ψ_z denotes the input angular velocity, E_d and ω_d represent the excitation drive mode's amplitude and frequency, R_{y1} and R_{y2} are the sense in-phase and anti-phase mode's displacement and quality factors respectively. Through sense mode displacement $y = y_1 + y_2$, and we can get, (2) and (3), as shown at the bottom of the next page.

Here

$$\varphi_{x2} = -tg^{-1}\left(\frac{\omega_{x2}\omega_d}{R_{x2}\left(\omega_{x2}^2 - \omega_d^2\right)}\right),$$

$$E_c = \frac{-2\psi_z\omega_d E_d}{m_x\sqrt{\left(\omega_{x2}^2 - \omega_d^2\right)^2 + \omega_{x2}^2\omega_d^2/R_{x2}^2}},$$

$$\varphi_{y1,2} = -tg^{-1}\left(\frac{\omega_{y1,2}\omega_d}{R_{y1,2}\left(\omega_{y1,2}^2 - \omega_d^2\right)}\right).$$

B. DETECTION SYSTEM

As shown in Figure 3, this is a gyroscope monitoring system diagram. Firstly, the differential amplifier obtains the drive frame displacement x(t), it can also be detected by driving the sense comb. Then, to meet the corresponding phase requirements, the AC drive signal $V_{dac}\mathrm{Sin}(\omega_d t)$ is delayed by 90 °, the pickup of $V_{dac}\mathrm{Sin}(\omega_d t)$ relies on a low-pass filter and a

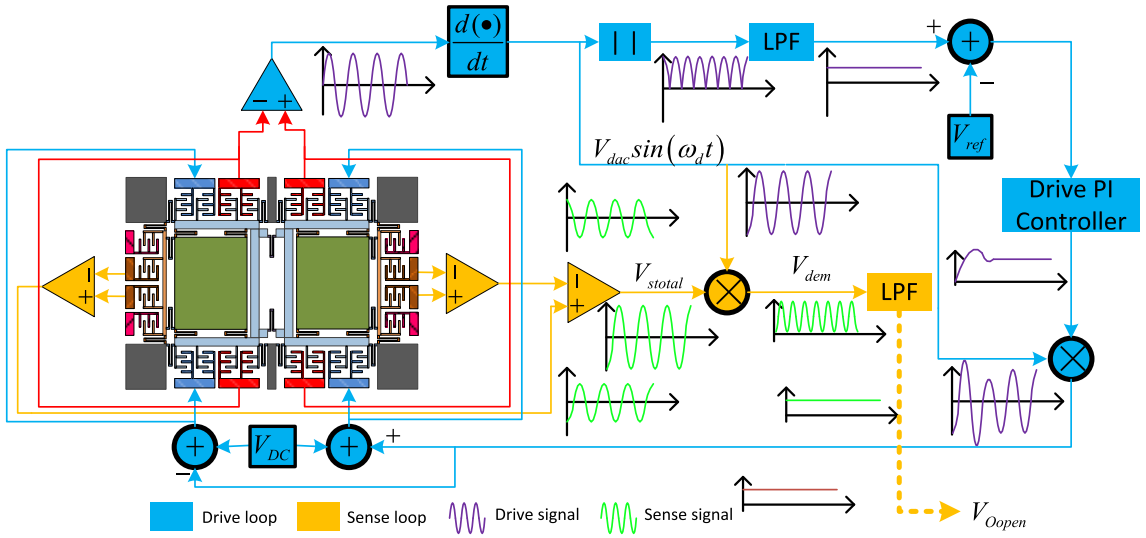

FIGURE 3. Gyro system schematic diagram.

full-wave rectifier, after that, the reference voltages V_{ref} and V_{dac} are compared. Next, by the integrator controller, the acting force of the drive mode is formed by superimposing the driving DC signal V_{DC} of $V_{dac}Sin(\omega_d t)$, and the control signal is also processed by it. The drive circuit and the induction circuit use the same interface, while the latter is open-loop. The differential detection amplifier generates the differential signal again by detecting the two masses' sense signals, the purpose of it is to generate the sense mode amplified signal V_{stotal}. Finally, the sense mode motion signal V_{Oopen} is generated in two steps: demodulation of $V_{dacSin}(\omega_d t)$ and low-pass filter. At the time V_{Oopen} is also used to sense the output signal of the open-loop (''yellow'' block in Figure 3).

III. COMPENSATION ALGORITHMS

A. LOCAL CHARACTERISTIC-SCALE DECOMPOSITION (LCD)

Local Characteristic-scale Decomposition (LCD) is an effective adaptive analysis technique for non-stationary signals [30]. It first defines a single component signal called intrinsic scale component (ISC), which has instantaneous frequency physical meaning. This method adaptively decomposes a series into the sum of some ISCs to obtain the original signal's complete time-frequency distribution. Here is a brief introduction to ISC.

Suppose any complicated series is comprised of diverse ISC products, each ISC is an independent component. For any

$$
\begin{aligned}
x(t) = {} & \frac{E_d/m_x}{\sqrt{\left(\omega_{x2}^2-\omega_d^2\right)^2+\omega_{x2}^2\omega_d^2/R_{x2}^2}}\sin(\omega_d t+\varphi_{x2}) + \frac{E_d\omega_{x2}\omega_d/m_xR_x}{\left(\omega_{x2}^2-\omega_d^2\right)^2+\omega_{x2}^2\omega_d^2/R_{x2}^2}e^{-\frac{\omega_{x2}}{2R_{x2}}t}\cos\left(\sqrt{1-1/4R_{x2}^2}\omega_{x2}t\right) \\
& + \frac{E_d\omega_d\left(\omega_{x2}^2/R_{x2}^2+\omega_d^2-\omega_{x2}^2\right)/m_x}{\omega_{x2}\sqrt{1-1/4R_{x2}^2}\left[\left(\omega_{x2}^2-\omega_d^2\right)^2+\omega_{x2}^2\omega_d^2/R_{x2}^2\right]}e^{-\frac{\omega_{x2}}{2R_{x2}}t}\sin\left(\sqrt{1-1/4R_{x2}^2}\omega_{x2}t\right) \qquad (2)
\end{aligned}
$$

$$
\begin{aligned}
y_{1,2}(t) = {} & \frac{E_c}{\sqrt{\left(\omega_{y1,2}^2-\omega_d^2\right)^2+\omega_{y1,2}^2\omega_d^2/R_{y1,2}^2}}\sin\left(\omega_d t+\varphi_{x2}+\frac{\pi}{2}+\varphi_{y1,2}\right) \\
& - \frac{E_c\left[\omega_{y1,2}\omega_d\sin\varphi_{x2}/R_{y1,2}+\left(\omega_{y1,2}^2-\omega_d^2\right)\cos\varphi_{x2}\right]}{\left(\omega_{y1,2}^2-\omega_d^2\right)^2+\omega_{y1,2}^2\omega_d^2/R_{y1,2}^2}e^{-\frac{\omega_{y1,2}}{2R_{y1,2}}t}\cos\left(\sqrt{1-1/4R_{y1,2}^2}\omega_{y1,2}t\right) \\
& + \frac{E_c\left[\omega_{y_{1,2}}\left(\omega_{y_{1,2}}^2-3\omega_d^2\right)\cos\varphi_{x_2}/\left(2R_{y_{1,2}}\right)+\omega_d\left(\omega_{y_{1,2}}^2/\left(2R_{y_{1,2}}^2\right)+\omega_{y_{1,2}}^2-\omega_d^2\right)\sin\varphi_{x_2}\right]}{\omega_{y1,2}\sqrt{1-1/4R_{y1,2}^2}\left[\left(\omega_{y1,2}^2-\omega_d^2\right)^2+\omega_{y1,2}^2\omega_d^2/R_{y1,2}^2\right]} \\
& \times e^{-\frac{\omega_{y1,2}}{2R_{y1,2}}t}\sin\left(\sqrt{1-1/4R_{y_{1,2}}^2}\omega_{y_{1,2}}t\right) \qquad (3)
\end{aligned}
$$

signal $f(t)$, the decomposed ISCs need to satisfy the following two conditions:

(I) In the entire data range, the minimum value is negative, and the maximum value is positive, there is a monotonic change between any two adjacent maximum and minimum values.

(II) In the entire data range, all extreme points are expressed as F_{u}, and the corresponding time is t_{u}, $u = 1, 2 \ldots N$, where N is the number of extreme values. The ratio of functional value $C_{\mathrm{u}+1}$ to $F_{\mathrm{u}+1}$ of the straight line $l_{\mathrm{u}}(y = \frac{F_{u+2}-F_u}{t_{u+2}-t_u}(x - t_u) + F_u)$ determined by any two adjacent maxima or minima points $(t_{\mathrm{u}}, F_{\mathrm{u}})$, $(t_{\mathrm{u}+2}, F_{\mathrm{u}+2})$ at the moment of $\mathrm{t_{u+1}}$ corresponding to the extremum $\mathrm{F_{u+1}}$ between the two remains unchanged. More generally, it is required to meet the following requirements:

$$qC_{u+1} + (1-q)F_{u+1} = 0, \quad q \in (0, 1) \tag{4}$$

$$C_{u+1} = F_u + \frac{t_{u+1} - t_u}{t_{u+2} - t_u}(F_{u+2} - F_u) \tag{5}$$

If a single component signal meets the above two conditions, it is called an intrinsic scale component (ISC). Condition (I) requires monotony between adjacent extremum points to ensure a single waveform. Condition (II) is to make the ISC waveform smooth and symmetrical. They guarantee that the ISC product has a unitary mode among any adjacent maximum and minimum values, locally coincident with the cosine curve, and the instantaneous frequency has physical meaning.

On the basis of ISC, a new signal decomposition method LCD is proposed. For complex signal $f\ (t)$ $(t > 0)$, LCD is used to decompose it, its brief introduction is as follows:

1) Determine the extreme point F_{u} of signal $f\ (t)$ and its corresponding time t_{u}, $u = 1, 2 \ldots N$, and set q in formula (4) to 0.5.

2) The straight line determined by all adjacent maximum (or minimum) points $(t_{\mathrm{u}},\ F_{\mathrm{u}})$, $(t_{\mathrm{u}+2},\ F_{\mathrm{u}+2})$ is $l_{\mathrm{u}}\ (y = \frac{F_{u+2}-F_u}{t_{u+2}-t_u}(x - t_u) + F_u)$, calculate the function value $C_{\mathrm{u}+1}$ of $t_{\mathrm{u}+1}$ at the time corresponding to the extreme point $F_{\mathrm{u}+1}$ between the two points according to the formula (5), that is the value of $L_{\mathrm{u}+1}$, wherein

$$L_{\mathrm{u}+1} = qC_{u+1} + (1-q)F_{u+1}, \quad u = 1, 2, \ldots N-2 \tag{6}$$

Since the subscripts k of the values of C_k and L_k are from 2 to $N-1$, we need to estimate the value of the endpoints $\mathrm{L_1}$ and $\mathrm{L_N}$. The common processing method is to extend the original data, similar to the endpoint extension method in EMD [31], [32]. By extending the extreme points, the extreme points (t_0, F_0), $(t_{\mathrm{N}+1}, F_{\mathrm{N}+1})$ are obtained. Let N be equal to 0 and $N-1$ respectively, then C_1, C_{N}, and L_1 and L_{N} can be obtained according to formula (6).

3) The mean curve (baseline) $DL_1\ (t)$ is obtained by fitting all $L_1, L_2 \ldots L_{\mathrm{N}}$ with cubic spline function.

4) Separate the baseline signal $DL_1\ (t)$ from the original signal $f\ (t)$.

$$I_1(t) = f(t) - DL_1(t) \tag{7}$$

If $I_1(t)$ satisfies conditions (I) and (II), it is an ISC, then output $I_1\ (t)$, and make $\mathrm{ISC_1} = I_1(t)$. Otherwise, take $I_1(t)$ as the original sequence $f\ (t)$, repeat the above steps u times until $I_{1,\mathrm{u}}(t)$ satisfies ISC conditions, that is:

$$I_{1,u}(t) = I_{1,u-1}(t) - DI_{1,u-1}(t) \tag{8}$$

$I_{1,\mathrm{u}}$ is the first ISC, recorded as $S_1(t) = I_{1,\mathrm{u}}(u)$. The ISC component criterion condition is the standard deviation method (SD) based on Cauchy criterion [33]–[35], and SD is defined as:

$$SD = \sum_{i=0}^{N} \left[\frac{\left| I_{iu}(t) - I_{i(u-1)}(t) \right|^2}{I^2_{i(u-1)}(t)} \right] \tag{9}$$

where N is the number of components. Generally, the value of SD is not more than 0.3, so the ISC component is more ideal. When $\mathrm{SD} \leq 0.3$, it is considered that $I_{1,\mathrm{u}}\ (t)$ satisfies the ISC component condition, and the iteration stops.

5) The S_1 component is separated from the original sequence f(t), and then the remaining signal $R_1\ (t)$ is obtained, that is:

$$R_1(t) = f(t) - S_1(t) \tag{10}$$

Then, $R_1(t)$ is regarded as the original sequence, and repeat the steps 1) to 5) until $R_{\mathrm{N}}\ (t)$ is a constant function or a monotonic function. Thus, the ISC components $S_1(t)$, $S_2(t)$, $\ldots S_{\mathrm{n}}(t)$ and the trend term $R_{\mathrm{n}}(t)$ are obtained successively.

6) The original signal $f\ (t)$ is decomposed to the sum of n ISCs and a trend term R_{n}(t).

$$f(t) = \sum_{i=1}^{n} S_i(t) + R_n(t) \tag{11}$$

At this point, LCD is completed.

B. PERMUTATION ENTROPY (PE)

After the output signal of the gyroscope is decomposed by LCD, several ISC components and a trend term $R_{\mathrm{n}}\ (t)$ are obtained. They contain different information, so it is necessary to distinguish and classify them and remove the noise component. Therefore, PE entropy is introduced here. PE is an effective algorithm that is sensitive to the time series and small changes in it. It is widely used to measure the complexity of the sequence [36], [37]. Here is a brief introduction to the PE algorithm [38].

Firstly, a time series $\{u(t), t = 1, 2, \ldots \mathrm{n}\}$ is reconstructed:

$$A = \begin{bmatrix} A(1) \\ \vdots \\ A(i) \\ \vdots \\ A(R) \end{bmatrix} = \begin{bmatrix} u(1) & u(1+\delta) & \cdots & u(1+(b-1)\delta) \\ \vdots & \vdots & \vdots & \vdots \\ u(i) & u(i+\delta) & \cdots & u(i+(b-1)\delta) \\ \vdots & \vdots & \vdots & \vdots \\ u(R) & u(R+\delta) & \cdots & u(R+(b-1)\delta) \end{bmatrix} \tag{12}$$

where A represents the reconstruction matrix with R components, δ is the delay time, b is the dimension, $i = 1, 2, \ldots R$, $R + (b-1)\delta = n$.

After that, each $A(i)$ is arranged in an increasing sequence, and the positions of elements are marked as follows according to $a_1, a_2, \ldots a_b$.

$$u(i+(a_1-1)\delta) \le u(i+(a_2-1)\delta) \le \ldots \le u(i+(a_b-1)\delta) \quad (13)$$

If the elements are of equal size, they are arranged according to their subscripts, that is:

$$\begin{cases} u(i+(a_m-1)\delta) = u(i+(a_l-1)\delta) \\ a_m < a_l \\ u(i+(a_m-1)\delta) \le u(i+(a_l-1)\delta) \end{cases} \quad (14)$$

So we can get a set of sequences $C(i) = (a_1, a_2, \ldots a_b)$ $i = 1, 2, \ldots R$. The index probability of each location is $P_1, P_2, \ldots P_R$. According to the form of entropy, PE value is calculated, which contains R different time series indexes, and then it is standardized to better compare the size:

$$H_p(b) = -\sum_{i=1}^{R} p_i \ln p_i \quad (15)$$

$$H_p = \frac{H_p(b)}{\ln b!} \quad (16)$$

The value of H_P reflects the complexity of the time series $u(t)$, the larger the value of H_P, the more chaotic the sequence $u(t)$ is.

C. SAVITKY-GOLAY FILTER

SG algorithm can filter out the noise while keeping the shape of the signal unchanged, that is, it protects the static features very well. It is a filtering method based on least square fitting, which is widely applied in signal denoising and data flow smoothing [39]–[42], its introduction is as follows.

Taking N as the length of the sample near the origin x, we get $2N+1$ sample points, that is to say, taking x as the center, we construct a window with a width of $2N+1$. Then, a polynomial of order n is constructed to fit it.

$$Q(z) = \sum_{i=0}^{n} d_i \cdot z^i \quad (17)$$

wherein, $-N \le z \le N$, $n \le 2N+1$.

Then, the fitting residual is:

$$\tau = \sum_{z=-N}^{N} (Q(z) - x(z))^2 = \sum_{z=-N}^{N} \left(\sum_{i=0}^{n} d_i \cdot z^i - x(z) \right)^2 \quad (18)$$

To obtain the minimum residual τ, the partial derivative of each parameter of τ is 0.

$$\frac{\partial \tau}{\partial d_n} = \sum_{z=-N}^{N} 2z^n \left(\sum_{i=0}^{M} d^i \cdot z^i - x(z) \right)^2 \quad (19)$$

$$\sum_{\mathrm{i}=0}^{M} \left(\sum_{z=-N}^{N} z^{n+i} \right) d_i = \sum_{z=-N}^{N} z^n x(z) \quad (20)$$

This window will always move to get all the original data fitting points, with the acquisition of the original data points, the noise data will be deleted from the normal data. In this paper, an SG filter is used to filter the mixed layer after the PE-LCD algorithm, and the useful components of the mixed layer signal are retained.

D. ANFIS ALGORITHM

Adaptive network-based fuzzy inference system was proposed by Jang and Roger Jang [26], [43]. It is a part of the neural fuzzy inference system, which combines neural network and fuzzy system, and has good learning and training ability and fuzzy inference function. Compared with other neural fuzzy systems, ANFIS is convenient and efficient, therefore, it is widely used in various fields. In this paper, ANFIS is used to build the temperature drift model of the gyroscope, and the structure principle of ANFIS is briefly introduced below.

In this paper, ANFIS based on Takagi Sugeno (T-S) fuzzy inference system is adopted, through training, it can realize nonlinear or linear mapping from input variable to output variable, and its adaptive network structure will be introduced [44].

As shown in Figure 4 is a multi-layer forward network, which consists of five layers in total, among which the block node represents the parameters that need to be adjusted.

First layer: the first layer is to make the input signal fuzzy, which is the membership function layer. Node i is a node with an output function.

$$D_i^1 = h_{Ai}(x) \quad i = 1, 2 \quad (21)$$

$$D_i^1 = h_{Bi}(y) \quad i = 1, 2 \quad (22)$$

Here, x, y is two variables, A_i and B_i are fuzzy sets, and D_i^1 is the membership function value of A_i and B_i, indicating the degree of x and y belonging to A_i and B_i. The shape of the membership functions h_{Ai} and h_{Bi} all depend on the front part parameters.

Second layer: the second layer is the regular intensity release layer. In this layer, the nodes are responsible for multiplying the input signals, each node's output represents the credibility of rules.

$$D_\mathrm{i}^2 = m_i = h_{Ai}(x) \times h_{Bi}(y) \quad i = 1, 2 \quad (23)$$

The third layer: normalize the strength of all rules, and calculate the normalized credibility value of the i-th rule at the i-th node.

$$D_i^3 = \overline{m}_i = \frac{m_i}{m_1 + m_2} \quad i = 1, 2 \quad (24)$$

The fourth layer: calculate the output of fuzzy rules. Each node is an adaptive node in this layer, and the i-th node's output can be expressed as:

$$D_\mathrm{i}^4 = \overline{m}_i T_i = \overline{m}_i (a_i x + b_i y + c_i) \quad (25)$$

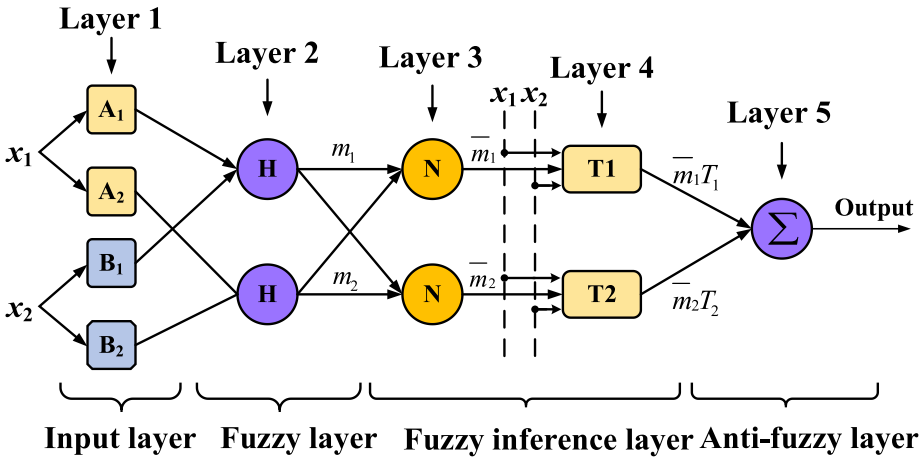

FIGURE 4. ANFIS system structure.

where, $\bar{m}_i$ indicates the third layer's output, $\{a_i, b_i, c_i\}$ is the parameter set of the node, which is called the subsequent parameter.

The fifth layer: it is a node with a fixed function to calculate the overall output of whole outlet signals:

$$D_i^5 = \sum \overline{m}_i T_i = \frac{\sum m_i T_i}{\sum m_i} \quad i = 1, 2 \tag{26}$$

Given the front part parameters, the ANFIS system's output is able to be described as a linear combination of the subsequent parameters:

$$f = (\overline{m}_1 x)\, a_1 + (\overline{m}_1 y)\, b_1 + (\overline{m}_1)\, c_1 + (\overline{m}_2 x)\, a_2 + (\overline{m}_2 y)\, b_2 + (\overline{m}_2)\, c_2 \tag{27}$$

Therefore, ANFIS can learn and adjust the parameters of the system's front part and subsequent part through the BP hybrid algorithm [26]:

1) First, determine the estimated value of the front part parameters, and then calculate to the fourth level, and then adjust the conclusion parameters with the least square method (LSE) and calculate the optimal estimation, which can be obtained from the above formula:

$$f = (\overline{m}_1 x)\, a_1 + (\overline{m}_1 y)\, b_1 + (\overline{m}_1)\, c_1 + (\overline{m}_2 x)\, a_2 + (\overline{m}_2 y)\, b_2 + (\overline{m}_2)\, c_2 = A \cdot X \tag{28}$$

Among them, the elements of column vector X constitute the subsequent parameter set $\{a_1, b_1, c_1, a_2, b_2, c_2\}$. Assuming that the input and output data pairs have n groups, and given the front part parameter, the bits of matrix A, X, f are $n \times 6$, 6×1, and $n \times 1$. In general, the quantity of samples is much larger than the number of unknowns ($n \gg 6$). Using the least square method, we can get the best estimate X^* of the subsequent parameter vector with the minimum mean square error, that is:

$$X^* = \left(AA^T\right)^{-1} A^T f \tag{29}$$

2) Due to the front part parameters are given, a linear combination of the subsequent parameters can be obtained. In terms of the subsequent parameters counted in the previous step, the error is calculated. BP algorithm is applied to transfer the error from the output to the input, and the front part parameters can be renewed by the gradient descent method, so as to change the shape of the membership function.

Simply put, in the hybrid algorithm, BP is applied to adjust the parameters of the front part, then the front part is calculated to the fourth layer, using LSE to distinguish the parameters of the back part. In the reverse phase, the error signal is transferred in the reverse direction, and the parameters of the front part are updated by the BP algorithm. When the current part parameters are fixed, the LSE method is the best method to identify the subsequent part parameters. The hybrid algorithm not only reduces the search space of BP but also raises the model's degree of accuracy [45].

E. PE-LCD-ANFIS PARALLEL MODEL

Figure 5 is the parallel processing model of PE-LCD-ANFIS proposed in this paper. The brief introduction is as follows:

a. Firstly, LCD is used to decompose the output signal of the gyroscope to obtain multiple ISCs and R. Then, PE is employed to analyze and calculate each component, based on the autocorrelation and complexity of the continuation, three different characteristic components are divided, namely noise output, mixed output, and drift output.

b. The signal in the noise output is chaotic, tending to white noise, and it can be removed directly since there is no useful component. Because the noise and the trend of temperature cannot be completely separated, the middle layer is a mixed output, which contains both noise and drift trends. It is necessary to extract drift trends and remove noise as much as possible, so SG smoothing is used. The denoising signal can be obtained by superposition of the drift output and the mixed output after SG processing.

c. Through SG, the drift component in the mixed output is extracted, but only contains a small amount of temperature characteristics. Different from the drift output, it belongs to the low-frequency drift part completely, and the output is

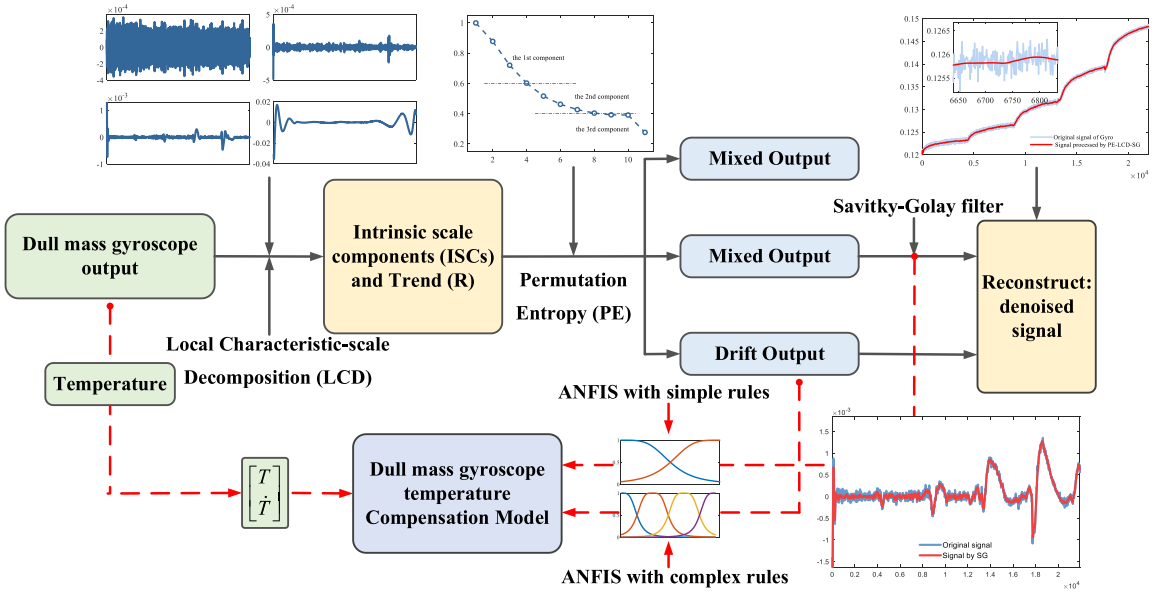

FIGURE 5. Flow chart of PE-LCD-ANFIS parallel model.

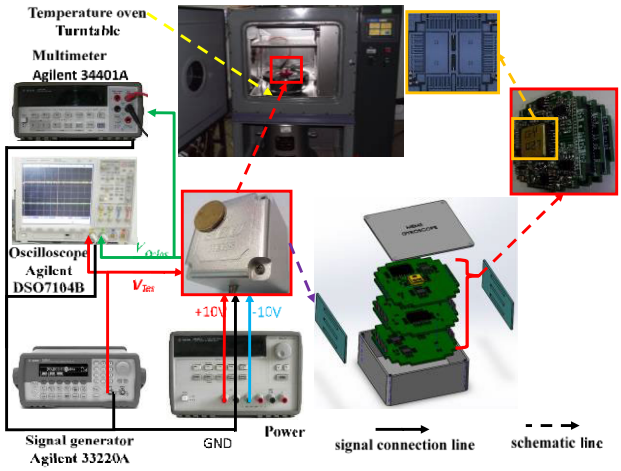

FIGURE 6. Equipment of temperature experiment.

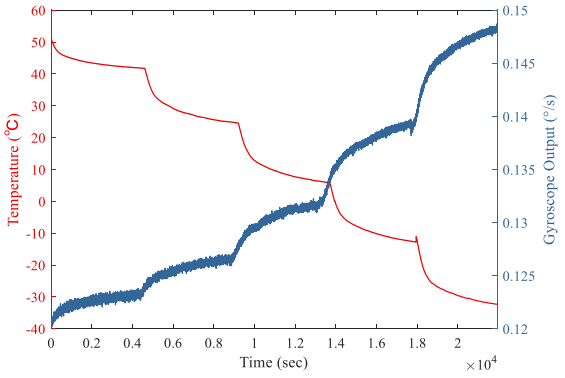

FIGURE 7. Experimental data1 for training.

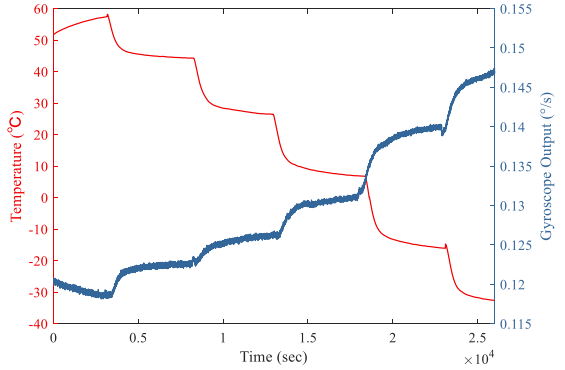

FIGURE 8. Experimental data2 for testing.

much more dependent on temperature change. To improve the efficiency and accuracy of the algorithm and further enhance the generalization ability of the model, ANFIS with simple rules was used for the mixed output and complex rules for the drift output. At the same time, the temperature sequence is processed to form a two-dimensional sequence of temperature and temperature change rate, which can better reflect the temperature situation. After training, the gyroscope temperature compensation model is obtained.

d. By reconstructing the processed mixed output and drift output, the final compensation signal can be obtained, which is the result of temperature error processing, in which high-frequency noise and low-frequency drift are eliminated.

IV. EXPERIMENTS AND ANALYSIS

A. EXPERIMENTAL APPARATUS AND PROCEDURE

Figure 6 shows the sample gyroscope and test equipment. The metal pins interconnect the mechanical structure and electronic signals of the monitoring circuit placed in the three PCBs. The rubber pad encapsulates the PCBs to prevent the structural chip and the PCBs from being vibrated and impacted, and then the packaged PCBs are placed in a metal case, the role of the metal case is to provide electromagnetic

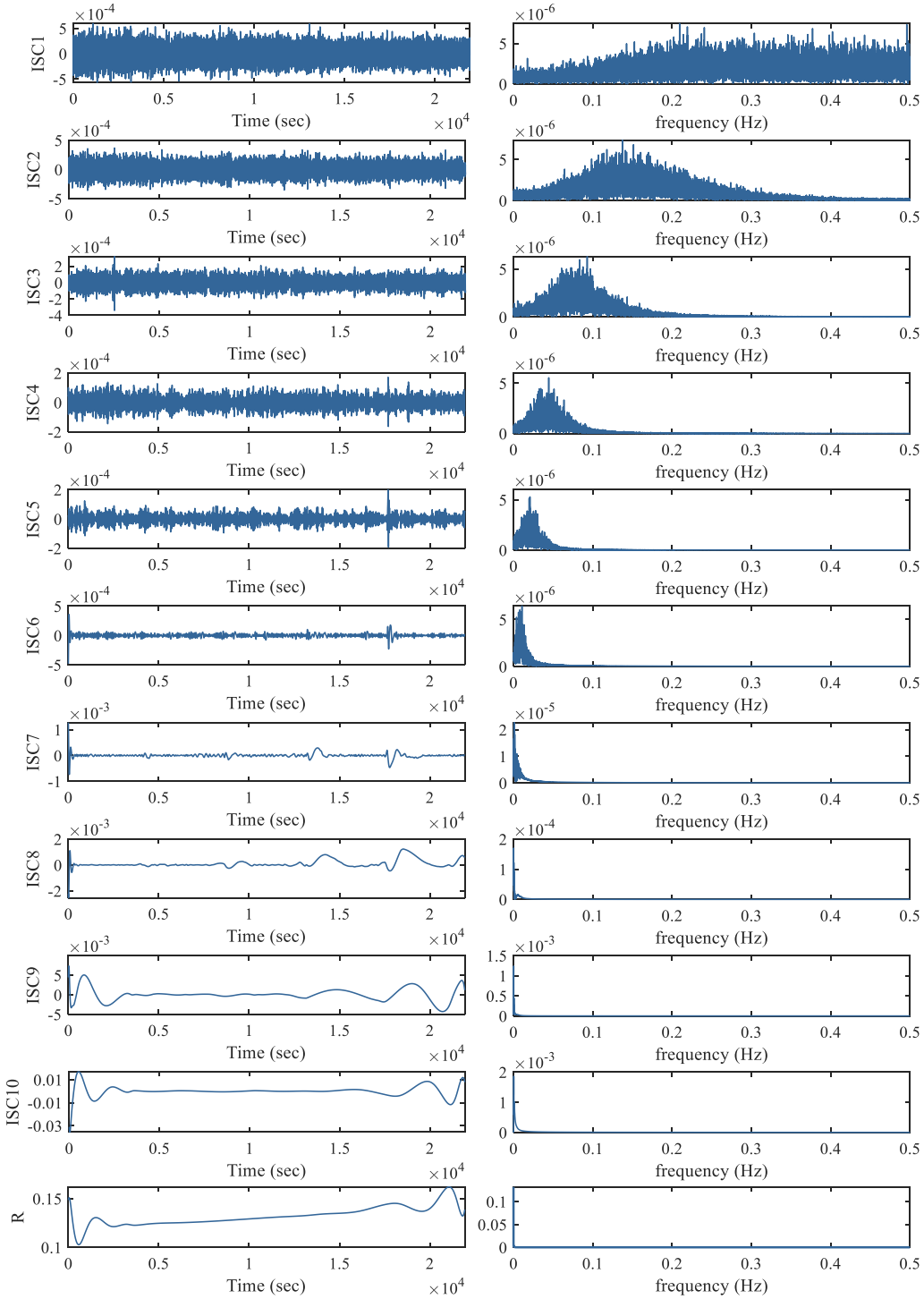

FIGURE 9. ISCs and R decomposed by Local characteristic-scale decomposition (LCD).

shielding and connect the "GND" signal. The functions of the three PCBs are different, the first block processes and interfaces with weak signals and connects the structural chip at the same time, the second block serves as the closed-loop of the driver, and the third block serves as the detection facility.

The test equipment includes GND and a power supply (Agilent E3631A) that generates ±10 V DC voltage. The test voltage V_{Tes} are generated by a signal generator (Agilent 33220A), the amplitude and phase of the observation and measurement signals are measured by a multimeter (Agilent 34401A) and an oscilloscope (Agilent DSO7104B).

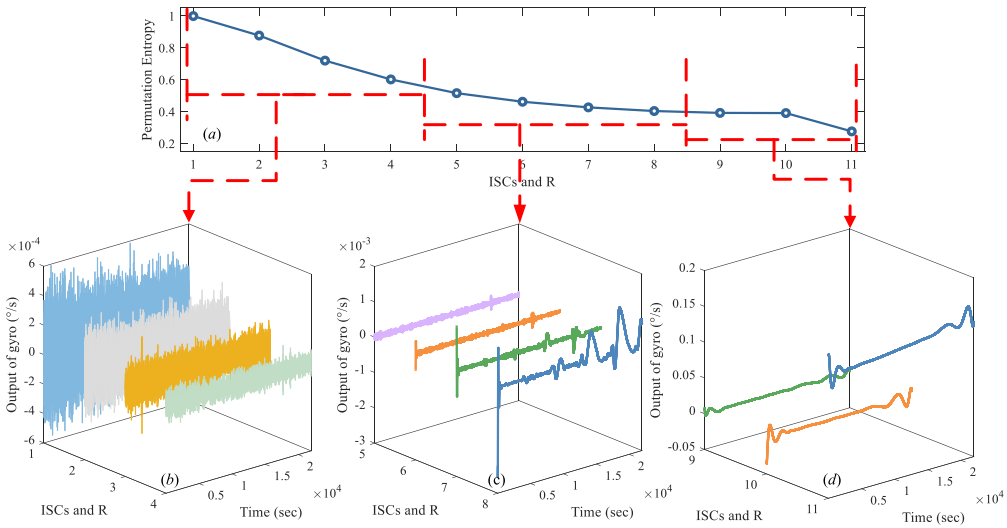

FIGURE 10. (a) Calculation results according to PE; (b) Pure noise outputs; (c) Mixed outputs; (d) Drift outputs.

The measurement of the actual width of the gyroscope and maintaining the environment over the entire temperature range is done through a turntable and a temperature oven.

The gyroscope is energized at room temperature for one hour, and then the oven temperature needs to be heated at high speed to 60 °C. To keep the temperature inside the gyroscope housing at 60 °C, the oven temperature needs to be maintained at 60 °C for one hour, this method can be proved correct by the thermal resistance value. So as to keep the gyroscope's internal temperature consistent with the oven's temperature and maintain stability, the initial temperature of the data collection needs to be positioned at 60 °C, at the time the oven temperature is set to stop for one hour after every 10 °C change. Finally, the test and all cooling steps are completed, and the sign is that the oven temperature has been maintained at −40 °C for at least one hour to make sure that the temperature in the MEMS gyroscope is stable.

After the measurement, we selected two sets of data for the temperature compensation experiment. One set was used as the training data of the model, namely the training set (Figure 7), and the other set was used as the testing set (Figure 8) to test the validity of the model. Besides, it can be seen from the experimental results that the output of the MEMS gyroscope has a clear response to the temperature change and the output changes with noises, so it is reasonable to create a drift compensation based on the temperature of the MEMS gyroscope model.

B. EXPERIMENTAL RESULTS

After the temperature experiment, the input and output data of the dull mass gyroscope are obtained. For the training set, we take the temperature range from 51 °C to −32 °C, as shown in Figure 7. It is obvious that, first, the dual-mass gyroscope's output contains a lot of white noise, and the noise amplitude and frequency change with the ambient temperature. This is because there are many sources of noise in the MEMS gyroscope. Second, the output changes with the temperature, the results show that the temperature drift is obvious, and the degree of temperature drift also changes, which is nonlinear and irregular.

Because of the above features, the serial processing method of direct filtering cannot be used, which will destroy the drift features of intermediate frequency or even low frequency, resulting in the reduction of compensation accuracy and effectiveness. Based on this, the LCD decomposition method is used to extract all kinds of features in the temperature series, and the framework of parallel processing is constructed.

Figure 9 is the result of LCD decomposition of the training set output and corresponding frequency spectrum, in which the number of decomposition layers value is set to 10, thus ten independent single component signal (ISC) components and a trend component are obtained. Each ISC is a signal component with a physical meaning. According to the frequency distribution, the frequency decreases from ISC1 to ISC10 to R, which represents the high-frequency noise and low-frequency drift component of the gyroscope output signal. The signal components obtained by decomposition are many, if each component is processed separately, the workload is huge and there will be large errors, therefore PE is used to judge each ISC component, and the regularity is found according to the complexity of time series, and they are classified.

As shown in Figure 10, the signal components of LCD are divided into three categories: noise, mixed and drift outputs. If the value of PE is greater than 0.6, it is considered as a complete interference component. The results show that the gyroscope noise tends to be pure white noise that can be removed directly. If the value of PE is less than 0.4, it is considered to be the drift component caused by the complete temperature factor and needs further treatment. If the PE value is between 0.4 and 0.6, it is considered to be the superposition of the temperature characteristic term and the noise, which represents

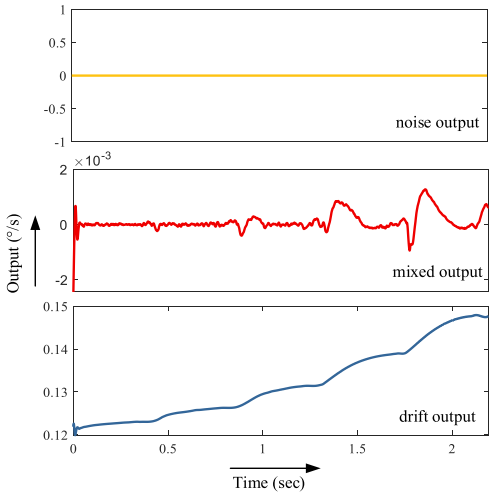

FIGURE 11. Noise component, mixed component after SG, and drift component.

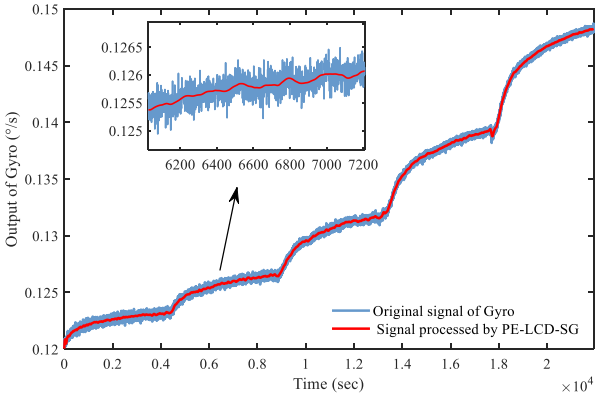

FIGURE 12. Denoised output (training set) and original signal.

the drift as well. It also needs further processing, because it cannot be completely separated, so SG is used to smooth it to retain the useful signals first. Overall, we deal with it from three aspects, and it is shown in Figure 11.

Reconstruct the drift output and mixed output after SG filtering to get the signal after denoising (Figure 12), comparing the denoising signal with the original signal, the processed PE-LCD and SG filtering method can remove the noise influence very well. The same process is then performed on the output of the testing set, and the denoising results are shown in Figure 13. And the next is to build the temperature compensation model.

Firstly, the temperature data of the training set are processed to obtain the two-dimensional sequence including temperature and temperature change rate, and the mapping relationship of two inputs and one output, which can better characterize the temperature, and all the sequences are normalized.

After that, two ANFIS models are established to construct the mixed output and the drift output respectively, this is because they contain different temperature characteristics. The mixed output has fewer drift components and gentle variation in amplitude, and still contains useless components,

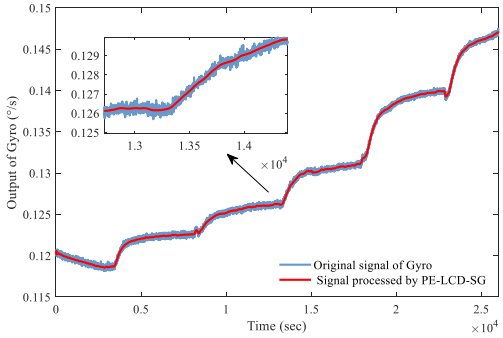

FIGURE 13. Denoised output (testing set) and original signal.

To prevent over-fitting of the model, simple rule ANFIS is used to train it as auxiliary compensation. The drift output belongs to the part with pure temperature characteristics and has a strong relationship between gyro output and temperature, which is the main concern part of temperature compensation. Therefore, the ANFIS with complex rules is adopted for training. Dual-ANFIS modeling compensation can reduce the computational effort and improve the accuracy and generalization ability of the algorithm.

Figure 15 shows the training and prediction process of ANFIS for drift output. The drift output has a high degree of nonlinearity, an ANFIS model with 16 fuzzy rules is constructed, that is, the temperature characteristic has four membership functions, and the temperature change rate characteristic has four membership functions. Through three iterations, 30 points are randomly selected for prediction, and the result is shown in Figure 15 (*a*), after 50 iterations, the result is shown in Figure 15 (*b*). After iterative training, it can be seen that ANFIS with complex rules has high training accuracy for drift output and fast convergence speed from Figure 15 (*c*).

The training and prediction process of ANFIS for mixed output is shown in Figure 15. The sequence is composed of ISCs in the middle layer with less temperature drift characteristics, therefore, the ANFIS model with 4 fuzzy rules is constructed for regression, that is, the temperature characteristics have corresponding 2 membership functions, and the temperature change rate characteristics have 2 membership functions. Similarly, 30 points are randomly selected for prediction and tested after 3 and 50 iterations, and the results are shown in Figure 15 (*a*) and Figure 15 (*b*) respectively. The ANFIS with simple rules has obvious training fitting effect on mixed output. and its iteration error is shown in Figure 15 (*c*).

After the training of the dual ANFIS model was completed by using the training set, the temperature compensation was carried out on the testing set and the compensation results were obtained by reconstructing the signals, as shown in Figure 16. It can be concluded that the parallel processing method of temperature error based on PE-LCD-ANFIS can effectively remove noise and drift.

Then, Allan analysis of variance was used to make a comparison. Allan is a standard performance analysis method of gyroscopes, it is a time series analysis method, which is applicable to evaluate every random noise coefficient and it

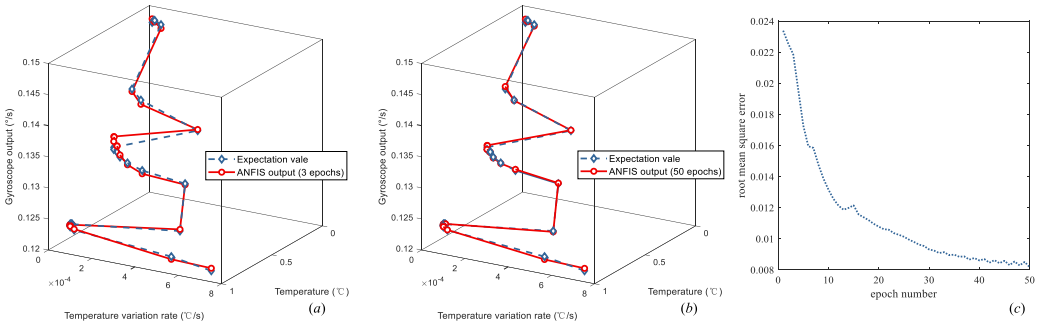

FIGURE 14. ANFIS of drift output (a) prediction test (3 epochs); (b) prediction test (50 epochs); (c) Iteration errors.

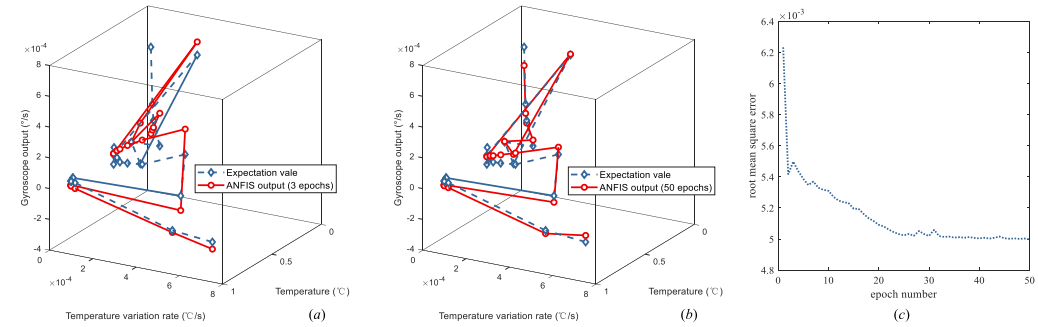

FIGURE 15. ANFIS of mixed output (a) prediction test (3 epochs); (b) prediction test (50 epochs); (c) Iteration errors.

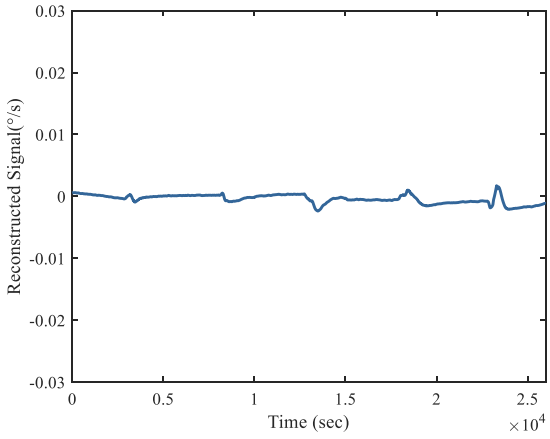

FIGURE 16. Gyro output signal (testing data) after compensation.

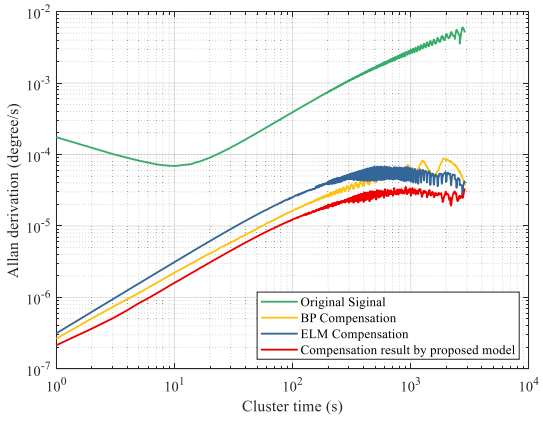

FIGURE 17. Allan analysis of variance and comparison.

has been widely used [46]. Figure 17 is the Allan variance curve of the gyro's output signal (testing set) and the processed signal by PE-LCD-ANFIS. At the same time, it is compared with the compensation results of other classical machine learning algorithms, compared with BP and ELM compensation, the performance index of the proposed model is better, and the effectiveness of the method is proved. Information can be obtained from the image: for the original signal, the random walk value of angular velocity is 1.744×10^{-4} °/s/$\sqrt{\text{Hz}}$, the bias stability value is 6.918×10^{-5} °/s, after processing by the proposed parallel processing model, they are 2.141×10^{-7} °/s/$\sqrt{\text{Hz}}$ and 2.141×10^{-7} °/s respectively, the performance has been greatly improved, and it proves that the parallel processing method has a good performance.

This paper adopted a software compensation method based on parallel processing, which has the characteristics of high efficiency, low cost. However, software compensation is not suitable in some cases. The gyroscope itself should be stable. If the hardware structure of the gyro is consumed or changes greatly, the processing algorithm needs to be adjusted accordingly, and the test data should be reprocessed and trained, this is the limitation. In future work, we will continue to research new efficient algorithms, further research on MEMS gyroscope structure itself at the same time, combining hardware compensation and software compensation to improve the stability of long-time temperature compensation.

V. CONCLUSION

In this paper, the temperature characteristics of the MEMS gyroscope and the methods of denoising and compensation of the gyroscope signal are studied. A new parallel processing method based on PE-LCD and ANFIS is proposed, which is a hybrid parallel algorithm. Due to the noise and drift of gyroscope signal are different under different temperature conditions, LCD is applied to extract the noise and drift respectively for different processing, and PE divides the decomposed ISCs and trend term into noise, mixed and drift output according to the complexity. On the one hand, it reduces the workload of signal processing and protects the static characteristics. On the other hand, it can optimize the ANFIS model: ANFIS with two different fuzzy rules is applied to predict the drift output and mixed output respectively. According to its characteristics, complex rules are used for drift output, and simple rules are used for mixed output, which not only improves the model accuracy and generalization ability but also greatly reduces the amount of calculation. The optimized dual ANFIS can compensate for the temperature drift well. After that, the temperature experiment is carried out, the results of Allan variance analysis show the effectiveness, and compared with previous algorithms, it has certain novelty and advantage.

ACKNOWLEDGMENT

(Huiliang Cao and Chong Shen contributed equally to this work.)

CONFLICTS OF INTEREST

The authors declare no conflicts of interest.

REFERENCES

[1] P. Doostdar and J. Keighobadi, "Design and implementation of SMO for a nonlinear MIMO AHRS," *Mech. Syst. Signal Process.*, vol. 32, pp. 94–115, Oct. 2012.
[2] D. Zhao, X. Liu, H. Zhao, C. Wang, J. Tang, J. Liu, and C. Shen, "Seamless integration of polarization compass and inertial navigation data with a self-learning multi-rate residual correction algorithm," *Measurement*, vol. 170, Jan. 2021, Art. no. 108694.
[3] H. Huang, R. Shi, J. Zhou, Y. Yang, R. Song, J. Chen, G. Wu, and J. Zhang, "Attitude determination method integrating square-root cubature Kalman filter with expectation-maximization for inertial navigation system applied to underwater glider," *Rev. Sci. Instrum.*, vol. 90, no. 9, Sep. 2019, Art. no. 095001.
[4] C. Shen, Y. Zhang, J. Tang, H. Cao, and J. Liu, "Dual-optimization for a MEMS-INS/GPS system during GPS outages based on the cubature Kalman filter and neural networks," *Mech. Syst. Signal Process.*, vol. 133, Nov. 2019, Art. no. 106222.
[5] J. Guerrero-Castellanos, H. Madrigal-Sastre, S. Durand, L. Torres, and G. Muñoz-Hernández, "A robust nonlinear observer for real-time attitude estimation using low-cost MEMS inertial sensors," *Sensors*, vol. 13, no. 11, pp. 15138–15158, Nov. 2013.
[6] I. P. Prikhodko, A. A. Trusov, and A. M. Shkel, "Compensation of drifts in high-Q MEMS gyroscopes using temperature self-sensing," *Sens. Actuators A, Phys.*, vol. 201, pp. 517–524, Oct. 2013.
[7] H. Cao, H. Li, J. Liu, Y. Shi, J. Tang, and C. Shen, "An improved interface and noise analysis of a turning fork microgyroscope structure," *Mech. Syst. Signal Process.*, vols. 70–71, pp. 1209–1220, Mar. 2016.
[8] Q. Fu, X.-P. Di, W.-P. Chen, L. Yin, and X.-W. Liu, "A temperature characteristic research and compensation design for micro-machined gyroscope," *Modern Phys. Lett. B*, vol. 31, no. 6, Feb. 2017, Art. no. 1750064.
[9] B. Yang, B. Dai, X. Liu, L. Xu, Y. Deng, and X. Wang, "The on-chip temperature compensation and temperature control research for the silicon micro-gyroscope," *Microsyst. Technol.*, vol. 21, no. 5, pp. 1061–1072, May 2015.
[10] X. Chen and C. Shen, "Study on temperature error processing technique for fiber optic gyroscope," *Optik*, vol. 124, no. 9, pp. 784–792, May 2013.
[11] C. Shen, J. Li, X. Zhang, J. Tang, H. Cao, and J. Liu, "Multi-scale parallel temperature error processing for dual-mass MEMS gyroscope," *Sens. Actuators A, Phys.*, vol. 245, pp. 160–168, Jul. 2016.
[12] G. Xu, W. Tian, and L. Qian, "EMD- and SVM-based temperature drift modeling and compensation for a dynamically tuned gyroscope (DTG)," *Mech. Syst. Signal Process.*, vol. 21, no. 8, pp. 3182–3188, Nov. 2007.
[13] H. Gu, X. Liu, B. Zhao, and H. Zhou, "The in-operation drift compensation of MEMS gyroscope based on bagging-ELM and improved CEEMDAN," *IEEE Sensors J.*, vol. 19, no. 13, pp. 5070–5077, Jul. 2019.
[14] X. Wen, D. Zhang, Y. Qian, J. Li, and N. Fei, "Improving the peak wavelength detection accuracy of Sn-doped, H_2-loaded FBG high temperature sensors by wavelet filter and Gaussian curve fitting," *Sens. Actuators A, Phys.*, vol. 174, pp. 91–95, Feb. 2012.
[15] B. Cui and X. Chen, "Improved hybrid filter for fiber optic gyroscope signal denoising based on EMD and forward linear prediction," *Sens. Actuators A, Phys.*, vol. 230, pp. 150–155, Jul. 2015.
[16] Z. Wu and N. E. Huang, "Ensemble empirical mode decomposition: A noise-assisted data analysis method," *Adv. Adapt. Data Anal.*, vol. 1, no. 1, pp. 1–41, Jan. 2009.
[17] A. Humeau-Heurtier, P. Abraham, and G. Mahe, "Analysis of laser speckle contrast images variability using a novel empirical mode decomposition: Comparison of results with laser Doppler flowmetry signals variability," *IEEE Trans. Med. Imag.*, vol. 34, no. 2, pp. 618–627, Feb. 2015.
[18] A. Venkitaraman, S. Chatterjee, and P. Händel, "On Hilbert transform, analytic signal, and modulation analysis for signals over graphs," *Signal Process.*, vol. 156, pp. 106–115, Mar. 2019.
[19] J. S. Cheng, J. D. Zheng, and Y. Yang, "A nonstationary signal analysis approach—The local characteristic-scale decomposition method," *Zhendong Gongcheng Xuebao/J. Vib. Eng.* vol. 25, no. 2, 2012, pp. 215–220, 2012.
[20] Z. Jinde, "Research on local characteristic-scale decomposition and its applications to machinery fault diagnosis," Ph.D. dissertation, College Mech. Vehicle Eng., Hunan Univ., Changsha, China, 2014.
[21] J. Zheng, H. Pan, S. Yang, and J. Cheng, "Generalized composite multiscale permutation entropy and Laplacian score based rolling bearing fault diagnosis," *Mech. Syst. Signal Process.*, vol. 99, pp. 229–243, Jan. 2018.
[22] Y. Li, G. Li, Y. Yang, X. Liang, and M. Xu, "A fault diagnosis scheme for planetary gearboxes using adaptive multi-scale morphology filter and modified hierarchical permutation entropy," *Mech. Syst. Signal Process.*, vol. 105, pp. 319–337, May 2018.
[23] X. Chen, "Application of a genetic algorithm Elman network in temperature drift modeling for a fiber-optic gyroscope," *Appl. Opt.*, vol. 53, no. 26, pp. 6043–6050, 2014.
[24] R. Song, X. Chen, C. Shen, and H. Zhang, "Modeling FOG drift using back-propagation neural network optimized by artificial fish swarm algorithm," *J. Sensors*, vol. 2014, pp. 1–6, Jan. 2014.
[25] S. Chong, S. Rui, L. Jie, Z. Xiaoming, T. Jun, S. Yunbo, L. Jun, and C. Huiliang, "Temperature drift modeling of MEMS gyroscope based on genetic-Elman neural network," *Mech. Syst. Signal Process.*, vols. 72–73, pp. 897–905, May 2016.
[26] J.-S. R. Jang, "ANFIS: Adaptive-network-based fuzzy inference system," *IEEE Trans. Syst., Man, Cybern.*, vol. 23, no. 3, pp. 665–685, Jun. 1993.
[27] O. Prakash and A. Kumar, "ANFIS modelling of a natural convection greenhouse drying system for jaggery: An experimental validation," *Int. J. Sustain. Energy*, vol. 33, no. 2, pp. 316–335, Mar. 2014.
[28] H. Cao, H. Li, Z. Kou, Y. Shi, J. Tang, Z. Ma, C. Shen, and J. Liu, "Optimization and experimentation of dual-mass MEMS gyroscope quadrature error correction methods," *Sensors*, vol. 16, no. 1, p. 71, Jan. 2016.
[29] H. Cao, R. Cui, and W. Liu, "Dual mass MEMS gyroscope temperature drift compensation based on TFPF-MEA-BP algorithm," *Sensor Rev.*, vol. 41, no. 2, pp. 162–175, May 2021, doi: 10.1108/SR-09-2020-0205.
[30] J. Zheng, J. Cheng, and Y. Yang, "A rolling bearing fault diagnosis approach based on LCD and fuzzy entropy," *Mechanism Mach. Theory*, vol. 70, pp. 441–453, Dec. 2013.
[31] J. Cheng, D. Yu, and Y. Yang, "Application of support vector regression machines to the processing of end effects of Hilbert–Huang transform," *Mech. Syst. Signal Process.*, vol. 21, no. 3, pp. 1197–1211, Apr. 2007.
[32] G. Rilling, P. Flandrin, and P. Goncalves, "On empirical mode decomposition and its algorithms," in *Proc. IEEE Workshop Nonlinear Signal Image Process. (EURASIP)*, vol. 3, Jun. 2003, pp. 8–11.
[33] N. E. Huang, Z. Shen, S. R. Long, M. C. Wu, H. H. Shih, Q. Zheng, N.-C. Yen, C. C. Tung, and H. H. Liu, "The empirical mode decomposition and the Hilbert spectrum for nonlinear and non-stationary time series analysis," *Proc. Roy. Soc. London. Ser. A, Math., Phys. Eng. Sci.*, vol. 454, no. 1971, pp. 903–995, Mar. 1998.

[34] N. E. Huang, M.-L.-C. Wu, S. R. Long, S. S. P. Shen, W. Qu, P. Gloersen, and K. L. Fan, "A confidence limit for the empirical mode decomposition and Hilbert spectral analysis," *Proc. Roy. Soc. London. Ser. A, Math., Phys. Eng. Sci.*, vol. 459, no. 2037, pp. 2317–2345, Sep. 2003.
[35] N. E. Huang and Z. Wu, "A review on Hilbert-Huang transform: Method and its applications to geophysical studies," *Rev. Geophys.*, vol. 46, no. 2, pp. 1–23, 2008.
[36] D. Cuesta–Frau, P. Miró–Martínez, S. Oltra–Crespo, J. Jordán–Nñez, B. Vargas, and L. Vigil, "Classification of glucose records from patients at diabetes risk using a combined permutation entropy algorithm," *Comput. Methods Programs Biomed.*, vol. 165, pp. 197–204, Oct. 2018.
[37] T. Ma, Z. Li, H. Cao, C. Shen, and Z. Wang, "A parallel denoising model for dual-mass MEMS gyroscope based on PE-ITD and SA-ELM," *IEEE Access* vol. 7, pp. 169979–169991, 2019.
[38] H. Cao, Z. Zhang, Y. Zheng, H. Guo, R. Zhao, Y. Shi, and X. Chou, "A new joint denoising algorithm for high-G calibration of MEMS accelerometer based on VMD-PE-Wavelet threshold," *Shock Vibrat.*, vol. 2021, pp. 1–16, Jan. 2021, doi: 10.1155/2021/8855878.
[39] Y. Guo, G. Li, H. Chen, Y. Hu, H. Li, L. Xing, and W. Hu, "An enhanced PCA method with Savitzky-Golay method for VRF system sensor fault detection and diagnosis," *Energy Buildings*, vol. 142, pp. 167–178, May 2017.
[40] Z. Wang, N. Yang, N. Li, W. Du, and J. Wang, "A new fault diagnosis method based on adaptive spectrum mode extraction," *Struct. Health Monitor.*, Jan. 2021, Art. no. 147592172098694, doi: 10.1177/1475921720986945.
[41] Z. Wang, W. Zhao, W. Du, N. Li, and J. Wang, "Data-riven fault diagnosis method based on EOSTI and convolutional neural network," *Process Saf. Environ. Protection*, vol. 149, pp. 591–601, May 2021, doi: 10.1016/j.psep.2021.03.016.
[42] Z. Wang, J. Zhou, W. Du, Y. Lei, and J. Wang, "Bearing fault diagnosis method based on adaptive maximum cyclostationarity blind deconvolution," *Mech. Syst. Signal Process.*, vol. 162, Jan. 2022, Art. no. 108018, doi: 10.1016/j.ymssp.2021.108018.
[43] E. S. Abdolkarimi, G. Abaei, and M. R. Mosavi, "A wavelet-extreme learning machine for low-cost INS/GPS navigation system in high-speed applications," *GPS Solutions*, vol. 22, no. 1, pp. 1–13, Jan. 2018.
[44] L. Zhang, Z. Xiong, J. Liu, and J. Xu, "Research on virtual gyro configuration of redundant MEMS system based on ANFIS," *Optik*, vol. 157, pp. 25–30, Mar. 2018.
[45] J. S. R. Jang, "Fuzzy modeling using generalized neural networks and Kalman filter algorithm," in *Proc. 9th Nat. Conf. Artif. Intell.*, Jul. 1991, pp. 762–767.
[46] L. Wang, C. Zhang, T. Lin, X. Li, and T. Wang, "Characterization of a fiber optic gyroscope in a measurement while drilling system with the dynamic Allan variance," *Measurement*, vol. 75, pp. 263–272, Nov. 2015.

HUILIANG CAO (Member, IEEE) received the Ph.D. degree in instrument science and technology from Southeast University, Nanjing, China, in 2014. From 2011 to 2012, he studied as a Research Ph.D. Student with the School of Electrical and Computer Engineering, Georgia Institute of Technology, Atlanta, USA. He is one of the Top Young Academic Leaders of the Higher Learning Institutions of Shanxi and the Young Academic Leaders of the North University of China. He is currently a Postgraduate Tutor and an Associate Professor with the School of Instrument and Electronics, North University of China. His research interest includes the areas of MEMS inertial devices.

WENQIANG WEI received the B.S. degree from the North University of China, Taiyuan, China, in 2019, where he is currently pursuing the M.S. degree with the School of Instrument and Electronics. His research interest includes MEMS sensor structure design.

LI LIU received the Ph.D. degree in instrument science and technology from Army Engineer University, Shijiazhuang, China, in 2018. She is currently a Lecture with The Army Infantry Academy of PLA, Shijiazhuang. Her research interests include sensor and equipment development.

TIANCHENG MA is currently pursuing the bachelor's degree with the School of Instrument and Electronics, North University of China, Taiyuan, China. His research interests include MEMS gyroscope signal conditioning and temperature compensation.

ZEKAI ZHANG is currently pursuing the bachelor's degree with the School of Instrument and Electronics, North University of China, Taiyuan, China. His research interest includes MEMS inertial devices.

WENJIE ZHANG is currently pursuing the bachelor's degree with the School of Instrument and Electronics, North University of China, Taiyuan, China. His research interests include denoising and compensating for MEMS gyroscopes.

CHONG SHEN received the Ph.D. degree in instrument science and technology from Southeast University, Nanjing, China, in 2013. He is currently an Associate Professor with the School of Instrument and Electronics, North University of China, Taiyuan, China. His research interests include the areas of MEMS inertial devices de-noising and inertial guidance system design.

XIAOMIN DUAN received the Ph.D. degree in instrument science and technology from the North University of China, Taiyuan, China, in 2015. He is currently a Postdoctoral Candidate with the School of Electronic Science and Engineering, University of Electronic Science and Technology of China, Chengdu, China. His research interests include inertial sensor and systems.